Aerosol Synthesized to Imitate Particles Produced by Combustion: Cloud Condensation and Water Uptake Properties

J.R.Snider[1], H.Wex[2], D.Rose[3], A.Kristensson[4], F.Stratmann[2], T.Hennig[2], S.Henning[2], A.Kiselev[2], M.Bilde[4], U.Dusek[3,*], G.Frank[3], A.Kiendler-Scharr[5], I.Lieberwirt[6], Th.F.Mentel[5], M.Petters[8], U.Pöschl[3], J.Schneider[7], R.Tillmann[5] and S.Walter[3]

[1] University of Wyoming, Department of Atmospheric Science, Laramie, USA

[2] Institute for Tropospheric Research, Department of Physics, Leipzig, Germany

[3] Max Planck Institute for Chemistry, Biogeochemistry Department, Mainz, Germany

[4] Department of Chemistry, University of Copenhagen, Copenhagen, Denmark

[5] Research Centre Juelich, ICG-II: Troposphere, Juelich, Germany

[6] Max Planck Institute for Polymer Research, Mainz, Germany

[7] Max Planck Institute for Chemistry, Particle Chemistry Department, Mainz, Germany

[8] Colorado State University, Department of Atmospheric Science, Ft. Collins, USA

* Now at Institute for Marine and Atmospheric Research, Utrecht University, Netherlands

Abstract

Four cloud condensation nuclei (CCN) instruments were used to sample size-selected test particles prepared at the Leipzig Aerosol Cloud Interaction Simulator (LACIS) facility. Included were two Wyoming static diffusion CCN instruments, the continuous-flow instrument built by Droplet Measurement Technology and the continuous-flow LACIS instrument. The aerosols were composed of ammonium sulfate, levoglucosan, levoglucosan and soot, and ammonium sulfate and soot. The goal of the study was two-fold: 1) To characterize, and compare, the water uptake and water nucleation properties of particles designed to mimic those produced by combustion, and 2) to compare a relatively larger number of measurements reported by four CCN instruments and a humidified tandem differential mobility system (27 experiments). The CCN comparison is quite encouraging - with few exceptions the CCN instruments reported critical supersaturations which agreed within the known uncertainties. Values of the CCN- and hygroscopicity-based estimates of the volume fraction also agree but for this aspect of the study the experimental uncertainties are larger and hence the agreement is not as impressive. We also analyze the Droplet Measurement Technology and Wyoming CCN measurements for evidence of size distribution broadening.

1-Introduction

Aerosol emitted into the atmosphere from combustion, and their effect on cloud properties and precipitation, has been the subject of research for several decades. A classic example is the observation of clouds contaminated by smoke emissions from sugar cane fires (Warner and Twomey, 1967). An analysis of that data set helped to solidify theory connecting aerosol abundance to both cloud reflection of solar radiation (cloud albedo) and precipitation (Twomey, 1977). Those achievements, and the many others that have followed, are now codified in the recognition that the combustion of both biomass and fossil fuel is one of the dominating sources of atmospheric particulate matter. This dominance is evident in the consideration given to particles generated by combustion in global aerosol models (Textor et al., 2006).

As is the case for all aerosol types, connecting the size and concentration of combustion particles to their effect on cloud albedo and precipitation requires additional information. Most revealing is the fraction of the dry particulate volume occupied by hygroscopic substances; material which promotes water uptake at relative humidities below saturation. In addition, hygroscopic materials also impact visibility (McMurry and Stolzenburg, 1989) and direct aerosol forcing of climate (Boucher and Anderson, 1995). Both hygroscopic and nonhygroscopic materials are recognized as significant components of particulate emitted from combustion sources (Andreae et al., 1988; Lightly et al., 2000).

Here we report on laboratory studies which used four cloud condensation nuclei (CCN) measurement systems, and an aerosol hygroscopicity measurement system, to characterize the condensed products of combustion. These studies, hereafter referred to as the Leipzig Experiment in November (LExNo), employed an apparatus which thermally condensed either ammonium sulfate or levoglucosan onto particles composed of soot. We report on measurements of the volume fraction of the particulate matter which is hygroscopic. The synthesized particles are thought to approximate particles emitted directly into the atmosphere from biomass burning (soot-levoglucosan particles) or that result from atmospheric processing of particulate derived from fossil fuel combustion (soot-ammonium sulfate particles) (Stratmann et al., 2009). Also investigated were particles composed solely of either ammonium sulfate or levoglucosan; analysis of these experiments allowed us to quantify CCN measurement error and the ability of three of the CCN instruments to retrieve the width of the test particle size

distributions. Our analysis of the LExNo data set is underlain by a robust, but simple, Köhler theory model which is used to calibrate the supersaturation in the CCN chambers, to derive the volume fraction of hygroscopic material and to quantify error propagation between measurements and derived quantities.

Other papers reporting on LExNo include the description of the particle generation apparatus and overall LExNo results (Stratmann et al., 2009), the analysis of aerosol chemical composition and hygroscopicity measurements (Henning et al., 2009) and the analysis of particle density and morphology (Kiselev et al. 2009).

2-CCN Instruments

Descriptions of the CCN instruments used during LExNo are published and will not be repeated here (Stratmann et al., 2004; Roberts and Nenes, 2005; Snider et al., 2006). However, we will discuss, and contrast, the physics underlying the production of supersaturated conditions in these instruments, the duration of time that aerosol is exposed to supersaturated conditions and the methodology used to relate the operational state of a CCN instrument to the occurrence of heterogeneous cloud droplet nucleation. Throughout this paper we will refer to this nucleation process as "activation." Figure 0 shows schematics of the three devices. The Copenhagen and Laramie groups both operated a Wyoming static diffusion CCN instrument (top panel), while the Leipzig and Mainz groups used the LACIS (bottom left panel) and the Droplet Measurement Technology (bottom right panel) continuous-flow CCN instruments, respectively.

In Figure 0 the vectors indicate the direction and magnitudes of the sensible and latent heat fluxes. For the static diffusion instrument, it is assumed that the fluxes are uniform in space (non-divergent) and that lateral wall effects are negligible. It is also assumed that fluxes do not vary with time (steady state assumption, see Katz and Mirabel, 1975). The uniform and steady flux assumptions lead to solutions of the one-dimensional heat and vapor mass diffusion equation. There are three important characteristics of this solution: 1) the temperature profile (in the vertical dimension) is approximately linear, 2) the vapor partial pressure profile is approximately linear (Katz and Mirabel, 1975), and 3) the saturation vapor pressure profile is non-linear. These characteristics lead to the quasi-parabolic supersaturation profile illustrated in Figure 0. The center of the chamber is illuminated with a laser and scattering produced by the activating particles is detected and related to CCN concentration via a calibration (Gras, 1995; Delene and Deshler, 2000; Snider et al., 2006).

Within the cylindrical Leipzig and Mainz flow tubes a relatively narrow aerosol stream is confined, by sheath airflow, to the tube centerline. This is in contrast with the situation in the static diffusion instrument where the aerosol sample is at rest and occupies the whole volume of the chamber. Focusing on the energy transport occurring at the tube centerline, and also perpendicular to it, the modelling study of Stratmann et al. (2004) demonstrates that the Leipzig instrument produces divergent fields of sensible and latent heat flux. From the LACIS inlet to about 20% downstream the aerosol stream experiences decreasing temperature, in response to the sensible heat flux divergence. Cooling drives an increase in relative humidity and this increase occurs in spite of the divergent latent heat flux. The magnitudes of the latent and sensible heat flux divergence do diminish with downstream distance and this is a consequence of the relaxation of the properties of the flow to the uniform boundary condition imposed by the tube wall. The model also shows that the maximum chamber supersaturation is produced approximately halfway down from the top of the tube. This relative humidity maximum increases with increasing humidity of the aerosol stream entering the top of the tube and with decreasing wall temperature. In practice, the former is held constant by a humidifier positioned upstream of the tube entrance.

Focussing now on the schematic of the Mainz instrument, we note that the latent and sensible heat fluxes are convergent along the tube centerline. This means that the aerosol flow stream is both heated, and humidified, as it moves down the tube. Two other aspects of the Mainz instrument are different from LACIS. First, there are three tube heaters positioned at the top (heater #1), the waist (heater #2) and bottom (heater #3) of the flow tube. These heaters, and the heater control system, are designed to produce the condition $T_1 < T_3 < T_2$ such that the topmost streamwise-temperature gradient, between heaters #1 and #2, is greater than the gradient between heaters #2 and #3. Second, the tube walls are wetted with a water handling system, which differs from the situation inside LACIS, where the tube wall is wetted by condensation. In the Mainz instrument the supersaturation along the tube centerline is predicted to reach a maximum slightly above the waist of the tube and below that point a smaller supersaturation is achieved. A similarity between Mainz and LACIS is the prehumidification that occurs prior to the entry of aerosol stream into the flow tube.

Time-dependent predictions of the chamber supersaturation, along the tube centerline (Mainz and Leipzig instruments) and halfway between the parallel plates of the Laramie

chamber, are presented in Figure 1. The computational methods used to generate these profiles are described in Stratmann et al. (2004) (Leipzig instrument), in Saxena et al. (1970) (Laramie instrument) and in Subramanian (2009) (Mainz instrument (HOW TO REFERENCE A WEB PAGE?)). Clearly the duration of time corresponding to the occurrence of the maximum chamber supersaturation differs over a broad range with the smallest value in the Leipzig CCN and the largest in the Laramie CCN. It is difficult to say if this relevant to LExNo, but we do speculate that an overprediction of the activating supersaturation of pure levoglucosan particles may stem from the relatively short time interval that the Leipzig and Mainz instrument expose the aerosol to the maximum chamber supersaturation (section 7).

3-Experimental Methods

The purpose of this section is to describe aspects of the LExNo experimentation germane to the CCN studies, including the preparation of the test aerosols, the calibration of the maximum chamber supersaturation, the measurement of the test particle's hygroscopicity and the supersaturation scanning strategy employed by investigators from Wyoming, Copenhagen and Mainz. A complete description of the LExNo setup can be found in Stratmann et al. (2009).

3.1-Particle Synthesis

Two different particle synthesis techniques were employed during LExNo: 1) Spray atomization of ammonium sulfate/water solutions, or levoglucosan/water solutions, followed by aerosol drying, charge neutralization, size selection and dilution. The mobility-equivalent dry diameter of the size-selected particles was varied between 35 and 95 nm (Vienna-type electrostatic classifier, 1-to-10 aerosol to sheath flow ratio). We refer to the two resulting aerosols as "pure ammonium sulfate" and "pure levoglucosan." In some experiments the test particle concentration was measured with a Model 3010 and a Model 3025 (TSI, Inc) condensation particle counter (CPC) and in some experiments only a Model 3010 CPC was employed. Hereafter, we will refer to the CPC concentration measurement as "*CN* ." 2) The second particle synthesis technique involved the thermal condensation of either ammonium sulfate, or levoglucosan, onto soot particles produced by spark discharge. Between the soot generation step, and the thermal condensation step, the option of compacting the soot particles by exposing them to 2-propanol vapor was exercised in some of the experiments. In either case the particles were size-selected in an electrostatic classifier before, and after, the thermal condensation step. The particles that were extracted from the second electrostatic classifier

(Vienna-type electrostatic classifier, 1-to-10 aerosol to sheath flow ratio), at a mobility equivalent diameter equal to 84 nm, were diluted prior to continuous monitoring by a Model 3010 CPC, a Model 3025 CPC and the CCN instruments. For particles prepared by either technique we assume that the measured mobility equivalent diameter approximates their mass equivalent diameter. The former was established in the second Vienna-type electrostatic classifier.

3.2-Calibration of the Maximum Chamber Saturation

Accurate determination of the maximum supersaturation achieved in the CCN chambers is an important objective of this work. This objective is challenging because thermal gradients are known to exist between the location where temperature is measured, within the wall of a CCN chamber, and the interior of the chamber (Snider et al., 2006; Lance et al., 2006). Furthermore, even if the air temperature and the H_2O vapor density could be measured at the location within the chamber where the supersaturation maximizes, measurement error can propagate into an unacceptable error in the derived supersaturation (Chýlek and Wong, 1998; Snider et al., 2006). We overcome these impediments by challenging the instruments with size-selected ammonium sulfate test particles of size sufficient to produce activation, and by correlating a surrogate representation of the maximum chamber supersaturation with the critical supersaturation of the activating particles[†]. The former is formulated in terms of static chamber wall temperatures (Katz and Mirabel, 1975; Snider et al., 2006), in terms of the LACIS wall temperature (Stratmann et al., 2004; Wex et al., 2006) and in terms of the stream-wise wall temperature gradient (Roberts and Nenes, 2005; Lance et al., 2006). We refer to the correlation between SS_c and the surrogate as the "chamber supersaturation calibration." Section 4 describes the Köhler theory model, which is integral to the calibration, Table 1 presents the outcome of those calibrations and Sections 5.1 and 5.2 discuss that result.

3.3-Hygroscopicity Measurements

Data from the high humidity tandem differential mobility analyzer (HH-TDMA) described by Hennig et al. (2005) was also analyzed. With one exception, discussed in Section 6.4, the HH-TDMA data was acquired simultaneous with the LExNo CCN measurements. The

[†] The supersaturation at the critical point SS_c, expressed in percent units, is defined in terms of the fractional relative humidity at the critical point (RH_c) by the relationship $SS_c = 100 \cdot (RH_c - 1)$.

fractional relative humidity of the measurements was typically 0.98 but varied from experiment to experiment by 0.002 fractional RH units.

3.4-Supersaturation Scanning Strategies

Each LExNo experiment lasted approximately 1 hour and for most of the duration of the testing intervals the four CCN instruments and the HH-TDMA sampled the test aerosol. Different supersaturation scanning strategies were employed with the supersaturation step equal to 0.01 SS units for the Copenhagen and Mainz instruments, and no smaller than 0.02 SS units for the Wyoming instrument.

4-The Köhler Model

Here we describe the development of a Köhler model which is capable of reproducing the prediction of an exact model, but which is also flexible enough for both the chamber supersaturation calibration and our analysis of the LExNo data set. Theoretical rigor is necessary since we use the Köhler model in analyses of activation and also in analyses of equilibrium water uptake. These objectives necessitate an accounting of the non-ideality of water-solute solutions at $RH = 0.98$ and also at the Köhler curve critical point where, in spite of the larger degree of solute dilution, the behavior of water-solute systems can depart substantially from ideality. Our other requirement is that the model can be initialized with either dry particle size or with relative humidity, and yield the coupled property without recourse to interpolation. On this point we note that the Aerosol Interaction Model (AIM, Wexler and Clegg, 2002) calculates solution composition corresponding to a prescribed relative humidity, but does not compute the relative humidity above a solution of prescribed composition. While this can be accomplished with a lookup table or by curve fitting we desired a simpler approach. A similar deficiency is seen in the model developed by Snider et al. (2003) which computes wet particle diameter corresponding to a prescribed relative humidity and dry particle size, but not the dry particle diameter corresponding to a wet particle diameter and a relative humidity. As we will see, the requirements of rigor and flexibility lead to approximation, yet we evaluate the extent of these limitations and show that they are small in comparison to measurement error.

COMMENT FROM MARKUS – THIS JUSTIFICATION IS NOT ADEQUATE, AND THERE IS NOTHING NOVEL IN THE EQUATIONS WHICH ARE PRESENTED BELOW. I AM THINKING ABOUT THAT CRITICISM.

4.1-The Working and Exact Köhler Models

Recognizing the demands of the chamber supersaturation calibration, and the LExNo analysis, we developed a Köhler model via the following path. We start with an exact formulation of the Köhler curve and use it to calculate relationships among RH, wet particle diameter (D_w) and dry particle diameter (D_d) for RH both below and at the Köhler curve critical point. Once established, the exact model is used to tune a parameter in the "working Köhler model." It is the working Köhler model that we exercise in the chamber supersaturation calibration and in analysis of the CCN and hygroscopic growth measurements performed during LExNo.

In the exact Köhler formulation we employ the expression developed by Mita (1979). This expression relates the fractional relative humidity over a solution droplet (RH) to three solution properties: water activity ($a(w)$), partial specific volume of water in solution ($v(w)$) and the air/solution interfacial tension ($\sigma(w)$).

$$RH = a(w) \cdot \exp\left(\frac{4M_w}{RT} \cdot v(w) \cdot \frac{\sigma(w)}{D_w(w, D_d)} \right) \tag{1a}$$

Here w is the weight fraction of solute in solution, M_w the molecular weight of water, R the universal gas constant, T the absolute temperature and D_w is the wet particle diameter. The dependence of the latter on solute weight fraction and dry particle diameter, shown explicitly in Equation 1a, is axiomatic if it assumed that the dry particle is a compact sphere, if all solute is dissolved and if the solution density is parameterized as a function of solute weight fraction ($\rho(w)$).

Since we employ data which expresses solution composition in terms of weight fraction, and also in terms of solute mole count per kilogram of water (molality), a second equation is needed to complete the exact Köhler formulism. Equation 1b describes the relationship among weight fraction, molecular weight of the solute (M_s) and solution molality (m)

$$m = \frac{w}{M_s \cdot (1 - w)} \tag{1b}$$

The formulism relies on the following sets of tabulated and parameterized solution property data: $a(m)$ (Low (1969a) for ammonium sulfate; Svenningsson et al. (2006) for levoglucosan), $\sigma(m)$ (Seinfeld and Pandis (1998) for ammonium sulfate; Svenningsson et al.

(2006) for levoglucosan) and $\rho(w)$ (Tang and Munkelwitz (1994)). For ammonium sulfate case the partial specific volume of water was derived via the $\rho(w)$ parameterization; however, for levoglucosan volume additivity was made. With that assumption the partial specific volume of water is equal to the specific volume of pure water (Brechtel and Kreidenweis, 2000). Equations 1a-1b were solved iteratively, yielding either a D_w at RH =0.98 (corresponding to a prescribed value of D_d) or a critical point relative humidity (RH_c) corresponding to a D_d. In summary, we refer to Equations 1a and 1b as the "exact Köhler model".

Our analysis uses a simplified Köhler model, the "working Köhler model", which we tuned to the exact model. For the tuning parameter we use a quantity which cloud and aerosol physicists may confuse for the vant Hoff factor (i). We demonstrate in the Appendix that the tuning parameter, symbolized by "j", should converge to the vant Hoff factor in situations where the water/solute solution is dilute, i.e. if the mole amount of water in the solution is much larger than the mole amount of solute. For common inorganic materials contained in particles which are deliquesced this occurs at RH values larger than approximately 0.95, and for many low molecular weight organics this relative humidity threshold is approximately 0.99 (Chan et al., 2008; Kreidenweis et al., 2008).

The working Köhler model is actually two different formulations. The first (Equation 2a) describes an equilibrium at RH =0.98 and contains the parameter j_e which was adjusted to force the best possible agreement with the exact model. The second formulation is for the situation at the critical point (Equations 2c is the derivative of Equation 2b set to zero) and contains j_c which was also adjusted to force the best possible agreement with the exact model.

$$RH = \exp\left(\frac{4M_w\sigma_w}{RT\rho_w}\cdot\frac{1}{D_w} - j_e\cdot\frac{\rho_s M_w}{\rho_w M_s}\cdot\frac{D_d^3}{(D_w^3 - D_d^3)}\right) \tag{2a}$$

$$RH_c = \exp\left(\frac{4M_w\sigma_w}{RT\rho_w}\cdot\frac{1}{D_w} - j_c\cdot\frac{\rho_s M_w}{\rho_w M_s}\cdot\frac{D_d^3}{(D_w^3 - D_d^3)}\right) \tag{2b}$$

$$0 = -\frac{4M_w\sigma_w}{RT\rho_w}\cdot\frac{1}{D_w^2} + 3D_w^2\cdot j_c\cdot\frac{\rho_s M_w}{\rho_w M_s}\cdot\frac{D_d^3}{(D_w^3 - D_d^3)^2} \tag{2c}$$

In sections 5 and 6 Equation 2a is used to describe the relationship among D_w, D_d, RH at a nominal measurement relative humidity (RH ~0.98) and measurement dry diameter, to derive an instrument-defined value of j_e and to assess the sensitivity of that j_e to experimental error in D_d and RH. Also, Equations 2b-2c is used to establish the chamber supersaturation calibration, to derive an instrument-defined value of j_c and to evaluate the sensitivity of that j_c to experimental error in D_d and RH_c. The working Köhler model has the advantage that it collapses the description of $a(w)$ into a simplified form containing a single adjustable parameter, and because this parameter is analogous to the van't Hoff factor familiar to many in the aerosol physics and cloud physics communities (Appendix A). As with the other single parameter Köhler model formulations (Hudson and Da, 1996; Petters and Kreidenweis, 2007; Wex et al., 2007) the working model can be solved forward and backward with a numerical equation solver without recourse to a lookup table or to curve fitting. It is this feature which facilitates our analysis of the LExNo data set. For solving the working model equations we employ an equation solver called "Newton" (IDL, ITT Visual Information Solutions, Boulder, CO, USA).

In Equation 1a, and in Equations 2a-2c, the temperature is fixed at a constant value (T=298.15 K) and ρ_s is set at 1769 kg/m^3 for ammonium sulfate and 1600 kg/m^3 for levoglucosan. Also, for Equations 2a-2c the surface tension is approximated as that of pure water (σ_w=0.0722 J/m^2 at T=298.15 K, Pruppacher and Klett, 1997) and the water density is assumed constant (ρ_w=997 kg/m^3). Because of the sensitivity of σ_w to temperature (Pruppacher and Klett, 1997), and since there is a difference between particle temperature in the instruments which cool the aerosol (Wyoming, Copenhagen and Leipzig) as opposed to those which warm it (Mainz), our assumption of one temperature for all instruments introduces a bias. By including a temperature-dependent interfacial tension in our exact model, and using estimates of the particle temperatures, we estimate this bias to be no larger than 0.05 SS_c units.

The four panels of Figure 2 compare the exact and working Köhler models. The basis for this comparison is a ratio formed by dividing the difference between the working and exact models by the prediction of the exact model. We refer to this ratio as the relative departure. Plotted in panels 2a and 2b is the relative departure for D_w, evaluated for both ammonium sulfate and levoglucosan at RH = 0.98 and formulated as $10^2 \times (D_{w,W} - D_{w,E}) / D_{w,E}$ where the

"W" and "E" subscripts indicate the working and exact models, respectively. In addition, panels 2c and 2d present the relative departure for RH_c, evaluated as $10^5 \times (RH_{c,W} - RH_{c,E}) / RH_{c,E}$. In all four panels the middle line represents to the parameter (j_e or j_c) which produces the best agreement between the working and exact models over the range of dry diameters employed during LExNo. Below and above this line are results obtained using tuning parameters which are 5% larger and 5% smaller than j_e (panels 2a and 2b), or tuning parameters which are 1% larger and 1% smaller than j_c (panels 2c and 2d).

Three conclusions are reached by examining Figure 2. First, the areas enclosed by the ±5% j_e lines (panels 2a and 2b), and the areas enclosed by the ±1% j_c lines (panels 2c and 2d), contain the "zero" value of the relative departure. This means that a value in the range $1.80 \leq j_e \leq 1.99$, in the case of ammonium sulfate (panel 2a), and in the range $0.82 \leq j_e \leq 0.90$, in the case of levoglucosan (panel 2b), produces exact agreement between the working and exact models. A similar conclusion is reached from an examination of panels 2c and 2b, but here a ± 1% range of j_c is displayed. In Section 6.4 we will demonstrate that a relative accuracy of either 5%, in the case of an instrument-derived value of j_e, or 1% in the case of an instrument-derived value of j_c is impossible to achieve experimentally. Second, we see that the two tuned values of j_c are smaller than that for levoglucosan and ammonium sulfate at infinite dilution; j_c=1 and j_c=3, respectively. This implies that the situation at the critical point is non-ideal. Third, we see that the value of j_c is larger than j_e; this is true for both solutes and reflects the larger degree of non-ideality in the more concentrated solution at RH = 0.98, compared to the situation at the critical point.

4.2–Validation of the Working Model

The levoglucosan working model was used to derive values of SS_c which were compared to the calculation shown in Figure 5a of Svenningsson et al. (2006). For ammonium sulfate our assessment of the water activity, based on Low (1969a), was decreased by 0.00005 activity units to compensate for a departure from the AIM activity model (Kreidenweis et al., 2005). This decrease is justified by the comparison between the activities from Low (1969a), and the AIM model, seen in Figure 4b of Kreidenweis et al. After making that activity

correction, which increased j_c to 2.38, a comparison was made to the AIM-based SS_c values reported in Kreidenweis et al. (their Table 2). In both of these model comparisons the agreement with the published SS_c was within 0.01 SS_c units. Furthermore, a sensitivity study demonstrated that that the approximation $v(w) \approx M_w / \rho_w$ leads to negligible differences over the range particle diameter of relevance to LExNo (35 to 95 nm).

5-Analysis Methods

This section presents the chamber supersaturation calibrations of the Laramie, Copenhagen and Mainz instruments (section 5.1), how those calibrations were used evaluate the activation properties of the LExNo aerosols (section 5.2) and discusses a distinction between the Leipzig instrument and the other three CCN instruments (section 5.2).

5.1-Chamber Supersaturation Calibration and its Error

Table 1 presents the chamber supersaturation calibrations developed for LExNo, demonstrating how the chamber wall temperature (T_w), the flow-parallel chamber wall temperature differences (ΔT), and the temperature-dependent "nominal" chamber supersaturation (S_{nom}; see Snider et al., 2006) are related to the maximum chamber supersaturation. The latter we view as a property of the CCN chamber, and symbolize as SS (the chamber supersaturation), to distinguish it from the particle-dependent property SS_c (the critical supersaturation).

Since each of the participating institutions have access to an electrostatic classifier for preparing calibration particles of known size and composition, the chamber supersaturation calibrations were developed at the investigator's home laboratories. Detailed descriptions of this development are provided in Wex et al. (2006), Rose et al. (2008), and in Bilde and Svenningsson (2004) for the Leipzig, Mainz, and Laramie/Copenhagen instruments, respectively. Ammonium sulfate was the material used for the chamber supersaturation calibration studies.

The final column of Table 1 presents the precision associated with the chamber supersaturation calibration relationship; here referred to as the "supersaturation error." Evaluation of this error requires repeated measurements at several dry test particle sizes, as described in Wex et al. (2006) and in Rose et al. (2008) for the Leipzig and Mainz CCN instruments, respectively. For the Laramie and Copenhagen instruments the supersaturation

error was derived via an analysis of the linear relationship between SS_c and S_{nom} (Snider et al., 2006).

5.2-Laramie, Copenhagen and Mainz Instruments

In the case of the Laramie, Copenhagen and Mainz instruments the evaluation of activation requires paired determinations of the concentration of CCN activating to form cloud droplets (CCN) and of the total particle concentration entering the CCN chamber (CN, see section 3.1). Further, these simultaneous concentration measurements must be acquired over a range supersaturation extending from negligible to complete activation of the test particles. We define the ratio of the paired CCN and CN concentrations as the active fraction and symbolize it by "A." As an example, we plot values of "A" reported by the Laramie instrument in the top panel of Figure 3. These data values are also overlain by error bars because each of the data points is an average of at least ten "A" values measured at a fixed value of SS spaced by at least 0.02 SS units (section 3.4). The figure reveals two active fraction plateaus; one at A~0.3 and the other at A~1. In the following paragraph we explain this behavior and how we account for it in the analysis of the LExNo data set. Since our approach is different from that described in Rosenørn and Bilde (????), we describe it detail.

The aerosols studied during LExNo were selected from two particle generation techniques, both of which produced a relatively broad size distribution (Section 3.1; also see Figure 3 of Stratmann et al., 2009). Of those particles which were selected from this broad initial size distribution a subset has larger size, by virtue of the fact that they were transmitted by an electrostatic classifier while carrying two, or more, units of electrical charge. Because these larger particles activate at a lower supersaturation, their presence obscures the activation behaviour of the physically smaller, but more numerous, unit-charge particles. Accounting for this is a three-step process. First, a particular value of the supersaturation is identified at the transition between the minor and major plateaus; we refer to this as SS^*. Second, values of "A" that plot in a narrow interval, extending from $SS = SS^*$ down to $SS = SS^* - \Delta SS$, were averaged to obtain a value for the active fraction which is representative of the right edge of the first plateau region. The top panel of Figure 3 shows the supersaturation averaging interval as a

vertical gray rectangle with width $\Delta SS = 0.06\%$ [‡]. Third, the average ($\overline{A}$, shown as a gray horizontal line) is used to correct the active fraction values in the following manner:

$$A(SS)_c = \frac{A(SS)_u - \overline{A}}{1 - \overline{A}} \tag{3}$$

Here, $A(SS)_c$ is the corrected activate fraction and $A(SS)_u$ is the uncorrected active fraction. In section 6.2 where we show more examples of active fraction plotted versus supersaturation we will only show the $A(SS)_c$ values and we will refer to this as the "active fraction." Finally, we note that values of $A(SS)_c$ that correspond to the minor plateau are negative; these values were set to zero for the curve fitting (discussed below) and for the graphical presentations.

Our assessment of the aerosol activation properties is based on a fit of the $A(SS)_c / SS$ data pairs. We chose a cumulative Gaussian function to fit the data

$$A(SS)_{fit} = \frac{C_2}{C_1 \cdot \sqrt{2 \cdot \pi}} \cdot \int_{-\infty}^{SS} \exp\left(-(SS' - C_0)^2 / (2 \cdot C_1^2)\right) \cdot d(SS') \tag{4}$$

Here C_2 is a scaling factor, C_1 is the standard deviation of the Gaussian function and C_0 defines the point where the function is equal to half its maximum value. For the Laramie, Copenhagen and Mainz instruments we take the value of C_0 to be the critical supersaturation of the test aerosol.

A fit of the corrected active fractions is shown in the bottom panel of Figure 3, and for contrast, the fit of the uncorrected active fraction values is shown in the top panel. From an examination of these fit lines and a comparison of the C_1 values it is apparent that the unit-charge particles (bottom panel) were distributed more narrowly than indicated by the fit of both charge categories (top panel). The correction described here was applied to all LExNo experiments which exhibited a substantial minor plateau.

[‡] Because of differences in the supersaturation scanning strategies, discussed in section 3.1, the ΔSS varied among instruments. We document both ΔSS and SS^*, in our data archive: http://www-das.uwyo.edu/~jsnider/lexno/FINAL.XLS . ADAM, DIANA AND JEFF WILL NEED TO SUPPLY VALUES OF ΔSS FOR THE ARCHIVE.

In summation, our analysis of the LExNo CCN data set is developed in terms of the critical supersaturation of the aerosol, which we will symbolize as SS_c and derive from a curve fit of $A(SS)_c / SS$ data pairs, and in terms of the width of the fitting function (C_1).

5.3-Leipzig Instrument

The determination of the SS_c by the Leipzig instrument was based on optical measurements of the wet particle diameter (D_w), made at the exit of the flow tube (Kiselev et al., 2005; Wex et al., 2006), simultaneous with a recording the LACIS wall (T_w). More detail on why T_w controls the supersaturation maximum achieved along the LACIS centerline can be found in Section 2 and in Wex et al. (2006). The particular T_w that is observed in association with activation (i.e., D_w increasing markedly with increasing T_w) was translated to a critical supersaturation via the calibration shown in Table 1.

6-Analysis of the LExNo Data Set

In this section we apply the calibrations and analysis tools, developed in Sections 4 and 5, to the CCN and hygroscopicity measurements that were made during LExNo. While our main focus is on particles synthesized to mimic those produced by combustion we first evaluate experiments which considered pure ammonium sulfate and pure levoglucosan particles.

6.1-Pure Ammonium Sulfate and Levoglucosan Particles

Table 2 shows that these particles were prepared by spray atomization of solute/water solutions, followed by aerosol drying, charge neutralization, size selection and dilution (Section 3.1). The selected dry particle diameters were 35, 50, 75 and 95 nm for the ammonium sulfate particles and 50, 75 and 95 nm for the levoglucosan particles. In the next two sections we present activation fractions and the critical supersaturations of these particles and also examine how well the Laramie, Copenhagen and Mainz instruments capture the width of the test particle size distribution function.

6.2-Cumulative Activation Spectra

Values of the active fraction are plotted versus supersaturation in the upper and lower panels of Figure 4. The coordinates of this presentation are discussed in sections 5.1 and 5.2. Furthermore only one of these coordinates is relevant to determinations of the SS_c coming from

the Leipzig instrument (Section 5.3), so we plot that particular SS_c value at an active fraction equal to 0.5.

Figure 4 reveals two general results of the LExNo CCN measurements. First, the top three panels shows the excellent agreement among the five independent assessments of SS_c for particles composed of ammonium sulfate - four CCN instruments and the working model initialized with the mobility-selected dry diameter. Table 2 presents the SS_c relative standard deviations for all of the pure ammonium sulfate experiments, demonstrating that this value is typically 0.02. The reader is reminded that ammonium sulfate was the material used in the home laboratories to establish the chamber supersaturation calibrations. Second, poorer SS_c agreement is seen in the bottom three panels of Figure 4 with the Mainz and Leipzig values plotting noticeably larger than either the working model or the Wyoming or Copenhagen values. This inconsistency is also reflected in the larger SS_c relative standard deviations reported for the pure levoglucosan experiments (Table 2).

6.3-Broadening of the Particle Size Distribution

Careful examination of Figure 4, for example a comparison of the fit lines shown in the two upper-left panels (top and bottom rows of Figure 4), suggests that the slope of the best fit line at active fraction = 0.5 is shallower for the Laramie instrument than it is for the Mainz instrument. This could mean that the former is broadening the test aerosol size distribution to a greater degree than the latter. Figure 5 addresses this hypothesis by plotting a derived size distribution width, based on fits of the active fraction data (section 5.2), versus the mobility equivalent dry particle diameter for both an ammonium sulfate (upper panel) and a levoglucosan (lower panel) experiment. The size distribution widths ($2\sigma_{50}$) were evaluated as the difference between dry diameters predicted by the working model when initialized with fractional saturation ratios corresponding to the SS_c minus one fitted standard deviation and SS_c plus one standard deviation. This calculation mimics the assessment of size distribution broadening previously reported for two Wyoming CCNs (Snider et al., 2006; see their Figure 10). One of those CCNs is the instrument operated by the Laramie group during LExNo. We conclude from this presentation that the width of the size distribution obtained from the two Wyoming-type instruments is approximately a factor of 2.5 times estimated width of size distribution. The difference between the Wyoming-type and Mainz instruments seen in Figure 5 is expected, but is

not yet explained mechanistically. It is thought that a factor contributing to the difference is the fact that the Mainz instrument employs an optical particle counter to discriminate and count activated particles while the Wyoming instrument relies on scattering from an ensemble of particles (activated and unactivated) to infer the activated particle concentration (Gras, 1995; Delene and Deshler, 2000; Snider et al., 2006).

6.4- Instrument-defined Values of j_c and j_e for Pure Ammonium Sulfate Particles

Here we demonstrate how the working model, combined with a measurements from a CCN instrument and a high humidity tandem differential mobility analyzer (HH-TDMA; Hennig et al., 2005) are used to derive instrument-defined values of j_e or j_c for size-selected pure ammonium sulfate particles. We also gauge how experimental error propagates into these estimates of j_e and j_c.

For this demonstration we pick a CCN measurement from LExNo and HH-TDMA measurements performed prior to LExNo (Hennig et al., 2005, final row of their Table 2). The mobility-selected dry particle diameters were 75 and 100 nm, for the CCN and HH-TDMA measurements, respectively.

Error in D_d is presumed to result from error in the control and measurement of the air flow rate through the electrostatic classifier used to select the test particles. Consistent with the nature of this error source we take the upper- and lower-limits on D_d to be 5% larger than, and 5% less than, the nominal values. For the SS_c error we use $\pm 0.02 \cdot SS_c$ (section 6.2). For the error in the fractional RH we apply the uncertainty reported by Hennig et al. (2005); i.e., RH -0.012 to RH +0.012.

Figure 6 presents the instrument-defined values of j_e or j_c (indicated by two crosses), derived by solving Equations 2b and 2c with measurements of SS_c and D_d and by solving Equation 2a with measurements of D_d, RH and D_w. A set of four points surrounding the nominal value is also evident. The coordinates of the four points were evaluated by solving for the "j" predicted by the working model when initialized with the perturbed measurements shown at each of the four vertices. We view the area of the resulting trapezoid as a domain that encompasses the likely occurrence of the instrument-defined j values. Further, we note that the uncertainties in these far exceed ambiguity stemming from the tuning parameter; recall that the

latter is no larger 5% (Section 4.1) while the half-height of the trapezoids in Figure 6 translate to a 15% error in the instrument-defined value of j_c and a 50% error in the instrument-defined value j_e. Based on this juxtaposition of the instrument-defined j values and the tuning parameters, and the uncertainties associated with the former, we conclude that refinement is needed before CCN-based assessments can be useful in constraining j_c to better than ±15% and that even greater improvement is needed on the side of relative humidity accuracy in the HH-TDMA. In spite of this pessimistic view of using either CCN or HH-TDMA to probe the properties of solution droplets, either subcritical or activated, we shall see that the measurement framework employed during LExNo does enable a robust assessment of the volume fraction of hydroscopic material contained in the soot-ammonium sulfate and soot-levoglucosan particles.

6.5-Instrument-defined j_c and j_e values for Pure Levoglucosan Particles

In these experiments we evaluate properties of particles composed solely of levoglucosan prepared at the dry diameters 50, 75 and 95 nm. We supplement the CCN-based assessment with measurements from the HH-TDMA which we use to derive j_e at RH ~0.98 (section 3.1). In addition, a data set consisting of D_d and the instrument-defined j_e, plus the working model (Equations 2b and 2c with the instrument-defined j_e substituted for j_c) was used to evaluate a SS_c corresponding to the HH-TDMA measurements. Results are shown in Figure 7.

For the smallest dry particle diameter, the left panel reveals an over prediction of the working model by the Mainz and Leipzig instruments, and by the Leipzig instrument at the other two dry particle sizes. The other CCN and HH-TDMA SS_c values were indistinguishable from the working model when the measurement uncertainties were considered (results not shown).

In the right panel the SS_c over predictions translate to an underprediction of j_c. Also in this panel, we show the error trapezoid (section 6.4), but for clarity this is only shown for Wyoming and Leipzig data points. It is apparent that that the discrepancy between the Leipzig j_c value and the working model cannot be explained in terms of measurement error in either D_d and SS_c and that this is true for all three D_d values. Although the error trapezoid is not shown for the Mainz instrument, consideration of that uncertainty, reveals that the low value

of j_c derived for that instrument at D_d =50 nm also cannot be explained in terms of error in D_d and SS_c.

6.6-Internally-Mixed Particles

The procedures developed for synthesizing internally-mixed particles consisting of soot and a hygroscopic material (ammonium sulfate or levoglucosan) are described in section 3.1. Two approaches, one based on CCN measurements and one based on HH-TDMA measurements are used in our analysis of that data set. For the first, we use averaged SS_c values. The SS_c values for the four instruments are shown in Figure 8 and the average SS_c and number of participating CCN instruments is annotated. The figure demonstrates that data is missing from the Laramie instrument after Experiment #63 and that the Leipzig instrument was unavailable for Experiments #73 to #80. It follows that most of the SS_c averages are from at least three instruments, yet about a quarter of the data set consists of averages derived from two instruments (Mainz and Copenhagen). An examination of Figure 8 reveals that departure from the experiment mean can exceed 0.1 SS_c units, especially for the Leipzig instrument, and that "typical" intra-experiment variability is approximately 0.05 SS_c units provided the Leipzig measurement is excluded from consideration. The error estimate of 0.05 SS_c units is consistent with the supersaturation error provided by the operator of the Laramie instrument, and is smaller than the supersaturation error for the Copenhagen instrument (Table 1). Based on this we conclude that the supersaturation error is bounding the intra-instrument variability seen in Figure 8, for the Laramie and Copenhagen instruments. Section 7 presents a discussion of the Leipzig and Mainz supersaturation errors the possibility that these estimates of SS_c were positively biased relative to the continuous-flow values.

The hygroscopic volume fraction (ε) we derive from the CCN measurements is based on the following equations.

$$RH_c = \exp\left(\frac{4M_w\sigma_w}{RT\rho_w} \cdot \frac{1}{D_w} - \varepsilon \cdot j_c \cdot \frac{\rho_s M_w}{\rho_w M_s} \cdot \frac{D_d^3}{(D_w^3 - D_d^3)} \right) \quad (5a)$$

$$0 = -\frac{4M_w\sigma_w}{RT\rho_w} \cdot \frac{1}{D_w^2} + 3D_w^2 \cdot \varepsilon \cdot j_c \cdot \frac{\rho_s M_w}{\rho_w M_s} \cdot \frac{D_d^3}{(D_w^3 - D_d^3)^2} \quad (5b)$$

We note the similarity of these equations to those developed for dry particles containing only one component (Equations 2b and 2c), and also point out that ε is defined as the hygroscopic volume (ammonium sulfate or levoglucosan) relative to the dry particle volume. Although Equations 5a and 5b are presented ad hoc, their justification follows from the recognition that the quantity $\varepsilon \cdot D_d^3$ represents the volume of hygroscopic material. Hereafter, we will refer to ε as the "volume fraction."

Equations 5a and 5b were solved simultaneously, with ε and the critical wet diameter as unknowns, subject to the constraint of an averaged SS_c, a D_d and material constants for either ammonium sulfate or levoglucosan (see Section 4.1). The derivation of volume fractions from the HH-TDMA measurements (RH, D_d and D_w) follows a similar approach but employs Equation 2a modified to include the volume fraction

$$RH = \exp\left(\frac{4M_w\sigma_w}{RT\rho_w} \cdot \frac{1}{D_w} - \varepsilon \cdot j_e \cdot \frac{\rho_s M_w}{\rho_w M_s} \cdot \frac{D_d^3}{(D_w^3 - D_d^3)} \right) \qquad (5c)$$

In Figure 9 we present the volume fractions and their error limits. It is apparent that the CCN and HH-TDMA volume fractions correlate and that much of the ε variability is driven by oven temperature. This temperature dependence stems from the fact that the saturation vapor densities of both levoglucosan and ammonium sulfate increase with increasing temperature, resulting in more vapor available for condensation, subsequent to quenching, at larger oven temperatures. The positive correlation is consistent with prior studies (e.g., Tao and McMurry, 1989) and is also discussed in the LExNo overview paper (Stratmann et al., 2009) and in a more complete analysis of the LExNo HH-TMDA than is presented here (Henning et al., 2009).

For the following discussion it is important to recall that the synthesized particles started out as mobility-selected soot aggregates which were either processed in a propanol compaction tube, or were not. We refer to the consequence of these two experimental options as propanol-compacted particles and uncompacted particles, respectively. Subsequent to this step the particles were passed though a propanol denuder and then into either the ammonium sulfate or the levoglucosan oven (Section 3.1).

Figure 9 demonstrates that the propanol-compacted particles have about the same, or even larger, volume fractions compared to the uncompacted particles. The former of these two observations is evident from the comparison of experiment #74 (propanol compacted) and

experiment #73 (uncompacted). For levoglucosan-coated soot particles the results are not as clear; mainly because propanol-compacted and uncompacted levoglucosan experiments are not available for comparable oven temperatures. Yet those experiments do suggest that the propanol-compacted particles have a *larger* volume fraction compared to uncompacted particles. This result is unexpected; we thought that propanol compaction would lower the surface area available for additional condensation and would therefore produce particles with a smaller volume fraction. The result suggests that the amount of condensation depends primarily on oven temperature, and that particle surface area is of secondary importance.

Another result from in Figure 9 is the systematic difference among the volume fraction in the middle-left panel; the most obvious being experiments #62, #63 and #73 with a volume fraction of approximately 0.6 and approximately 0.3 coming from the HH-TDMA and CCN data sets, respectively. While it is true that analyzing the HH-TDMA data with a Köhler model for ammonium hydrogen sulfate (NH_4HSO_4), which was observed in these particles (Henning et al., 2009), does decrease the ε, a comparable decrease is also obtained for the CCN-based volume fractions. Rather than show that result, we draw the reader's attention to the error limits in Figure 9. For the HH-TDMA values the error limits were derived by perturbing the working Köhler model with a fractional relative humidity above and below the nominal value (RH, section 3.3). The range of this perturbation is from RH -0.012 to RH +0.012 (Hennig et al. (2005)). With this measurement error we see an overlap between the lower-limit of the HH-TDMA calculation and the value of ε derived using the averaged SS_c. This result reinforces the assertion made in section 6.4, i.e., that a RH measurement uncertainty of one part in a hundred propagates into a 50% error in parameters which are multiplicative in the exponential representation of the water activity in Equation 5c.

7-Discussion of the Continuous-flow and Static-diffusion CCN Results

LExNo brought together operators of the two most common instruments deployed for investigations CCN properties. These two instruments, manufactured by the University of Wyoming and Droplet measurement Technology, were operated with the LACIS instrument (in CCN mode) and the high humidity tandem differential mobility analyzer. Laboratory investigations of both pure and internally-mixed particles were conducted at the LACIS facility in November 2005 during LExNo.

It is tempting to attribute the significant departures in Figure 7 to the relatively short time interval that the continuous-flow instruments (Leipzig and Mainz) expose particles to the maximum chamber supersaturation. Figure 2 shows the calculations which motivated this line of inquiry. If our conjecture is correct, then it also follows that the continuous-flow instrument's supersaturation calibration *underestimates* the thermal forcing (Table 1) necessary to grow levoglucosan particles to their critical size in the time that is allotted; otherwise we see no reason why the chamber calibration would be incorrect for levoglucosan particles. Figure 8 shows two conflicting pieces of information which helps to resolve this issue. First, the middle-left panel shows the Leipzig instrument is overestimating relative to the static chambers (and Mainz) in experiments with internally-mixed particles containing ammonium sulfate. This suggests that the departures seen for levoglucosan (Leipzig instrument, left panel of Figure 7) are caused by a bias in the supersaturation calibration, and that they are not attributable to retarded growth of levoglucosan particles relative to ammonium sulfate particles. Second, a few of the soot-levoglucosan experiments (#49 and #86, Figure 8) do exhibit the behavior as seen in left panel of Figure 7; i.e. significantly larger SS_c values for the both continuous-flow instruments relative to that reported by one of the static diffusion instruments. Given the first of these observations a categorical conclusion about retarded particle growth of levoglucosan particles, in the Leipzig instrument, is not defensible. Since the Mainz instrument plots closer to the static chambers in Figures 7 and 8, a conclusion is also not defensible for this CCN.

The supersaturation error (Table 1) is a factor which weights in our ability to conclude with regard to a SS_c overestimation by the continuous-flow instruments relative to the static-diffusion chambers. Readers will recall from section 6.5 that an accounting of the supersaturation error gave an indication of SS_c overestimation in the case of the Mainz measurements, made at the smallest pure levoglucosan diameter, and overestimation in the case of the Leipzig instrument at all three levoglucosan diameters. Here we repeat that analysis using the measurements of internally mixed particles, presented in Figure 8. Although the supersaturation error limits are not shown Figure 8, an examination of that error reveals that their magnitude (typically ±0.04 and ±0.02 SS_c units for the Leipzig and Mainz instruments, respectively) is not sufficient to account for the positive departure between continuous-flow and static-diffusion determinations of SS_c seen in experiments #49 and #86. On the other hand, the

supersaturation error is sufficient to explain the other continuous-to-static departures, some of which go the negative direction (e.g., experiment #50). From this analysis, which compares a suspected SS_c bias to the statistical error associated with the supersaturation calibration, it is difficult to conclude affirmatively that the continuous-flow SS_c values were overestimated relative the static-diffusion values.

9-Conclusions

A significant result of these studies is the level of agreement between the critical supersaturations derived from the CCN instruments, from the HH-TDMA measurements and from theory via measurements of dry particle diameter. For the five experiments which examined pure ammonium sulfate particles in the diameter range 35 to 95 nm this agreement is evident in the relative standard deviations shown in the top row of Table 2, and in the presentation of one of these experiments made in the top three panels of Figure 4. Similar agreement was found between the two static diffusion CCN assessments of the SS_c for pure levoglucosan particles, and with the critical supersaturation derived from HH-TDMA measurements. Taken together, these results support the conclusion that levoglucosan solutions, both at RH =0.98 and at activation, do not behave ideally. This is consistent with the water activity and surface tension parameterizations reported by Svenningsson et al. (2006), but since the upper-limit error for the Wyoming instrument nearly touches the value $j_c = 1$ (Figure 7 right panel) we cannot discount the possibility of ideal solution behavior. Prior studies of the activation of pure levoglucosan in static thermal gradient chambers concluded that ideal behavior could be assumed (Svenningsson et al., 2006; Rosenørn and Bilde, ????). Figure 7 also illustrates a discrepancy among determinations of the critical supersaturation coming from the static-diffusion and continuous-flow instruments.

By conducting parallel measurements with five instruments, LExNo made it possible for us to report on the measurement error inherent to a single-instrument determination of SS_c and to also explore the degree to which static-diffusion CCN instruments broaden the input size distribution, both relative to the Mainz instrument and relative to electrostatic classifier theory. The relative standard deviations which we report for 22 LExNo experiments (Table 2) indicate that the SS_c variability is roughly ±0.05 SS_c units, provided one ignores an overestimate suspected to result from the relatively short processing time in the continuous-flow instruments.

With regard to broadening, we conclude that there is little evidence for this occurring in the Mainz instrument and that the static diffusion CCN broadens by a factor 2.5 compared to the width of the input size distribution.

Our final two conclusions are cautionary. First, LExNo was designed to maintain the test aerosol population constant for approximately one hour. It is thus likely that applications which require time resolution better than one hour will be subject to SS_c error larger than what we document here. Second, because of limitations in our understanding of how thermodynamic state varies within the CCN instruments, we chose not to account for a substantial bias (±0.05 SS_c units, section 4.1) resulting from suspected differences in particle temperature among the four CCN instruments. Accounting for this bias should be an objective of future CCN comparison studies.

Appendix

Here we consider a spherical binary liquid solution consisting of water and dissolved solute. We demonstrate that the quantities j_e or j_c approximate the vant Hoff factor (i) in the limit where the mole amount of water in the solution is large relative to the mole amount of solute.

Water activity for a binary system can be expressed in terms of the mole amounts of water and solute (n_1 and n_2, respectively) and a vant Hoff factor (i) (see, for example, McDonald (1953)).

$$a_1 = \frac{n_1}{n_1 + i \cdot n_2} \qquad \text{(A1)}$$

Equation A1 arranges to Equation A2

$$\frac{1}{a_1} = 1 + i \cdot \frac{n_2}{n_1} \qquad \text{(A2)}$$

Assuming water and solute contribute to the volume of the aerosol solution as pure components (volume additivity assumption), and assuming that the dry aerosol particle is spherical and compact, the mole amount of water carried by a solution droplet of diameter D_w is

$$n_1 = \frac{\pi}{6} \cdot \frac{\rho_1}{M_1} \cdot \left(D_w^3 - D_d^3\right) \qquad \text{(A3)}$$

Here D_d is the diameter of the dry aerosol particle and ρ_1 and M_1 are the density and molecular mass of water. Evoking the spherical and compact assumption again, the mole amount of dry aerosol material is

$$n_2 = \frac{\pi}{6} \cdot \frac{\rho_2}{M_2} \cdot D_d^3 \qquad \text{(A4)}$$

Combining (A2), (A3) and (A4), the water activity can be described in terms of the vant Hoff factor, material constants and the two diameters

$$a_1 = \frac{1}{1 + i \cdot \frac{\rho_2 \cdot M_1}{\rho_1 \cdot M_2} \cdot \frac{D_d^3}{\left(D_w^3 - D_d^3\right)}} \qquad \text{(A5)}$$

Assuming the second term in the denominator is small relative one and making a Taylor series expansion of the right side of Equation A5, the relationship simplifies to Equation A6

$$a_1 = 1 - i \cdot \frac{\rho_2 \cdot M_1}{\rho_1 \cdot M_2} \cdot \frac{D_d^3}{\left(D_w^3 - D_d^3\right)} \qquad \text{(A6)}$$

The fractional relative humidity over the solution droplet (RH) is the product of water activity and the Kelvin effect. For the latter we assume negligible interaction between solution composition and surface tension (σ_w) and negligible interaction between solution composition and water partial specific volume (see Section 4.1). With these assumptions the Köhler Equation becomes

$$RH = \left(1. - i \cdot \frac{\rho_2 \cdot M_1}{\rho_1 \cdot M_2} \cdot \frac{D_d^3}{\left(D_w^3 - D_d^3\right)}\right) \cdot \exp\left(\frac{4 M_w \sigma_w}{\rho_1 R T D_w}\right) \qquad \text{(A7)}$$

Here R is the universal gas constant, M_w is the molecular weight of water, σ_w is the water surface tension and T is absolute temperature. Equation A7 can be further approximated by expressing the water activity in Equation A7 as an exponential

$$RH = \exp\left(\frac{4 M_w \sigma_w}{\rho_1 R T D_w} - i \cdot \frac{\rho_2 \cdot M_1}{\rho_1 \cdot M_2} \cdot \frac{D_d^3}{\left(D_w^3 - D_d^3\right)}\right) \qquad \text{(A8)}$$

The similarity between Equation A8 and Equations 2a and 2b means that quantities j_e or j_c approximate the vant Hoff factor (i). The main assumption is that second term in the dominator of Equation A5 is small relative to one; this implies that the solution is dilute ($n_1 >> i \cdot n_2$).

Table 1 – CCN instruments, chamber supersaturation calibration and supersaturation error

Type	Operating Institution	Supersaturation Calibration	Supersaturation Error
Wyoming Static Diffusion [a] (SN: CCNC-100A-104)	Dept. of Atmospheric Science University of Wyoming, Laramie, USA	[b] $SS = 0.64 \cdot SS_{nom}$	$\delta_{SS} = 0.05 \cdot SS$
Wyoming Static Diffusion [a] (SN: CCNC-100A-107)	Dept. of Chemistry University of Copenhagen, Denmark	$SS = 0.71 \cdot SS_{nom}$	$\delta_{SS} = 0.18 \cdot SS$
[c] DMT Continuous Flow [a] (SN: 02/05/0011)	Max Planck Institute for Chemistry Mainz, Germany	[d] $SS = 0.077 \cdot \Delta T - 0.0052$	$\delta_{SS} = 0.03 \cdot SS$
[e] LACIS Continuous Flow [a] (SN: Not Applicable)	Leibniz Institute for Tropospheric Research Leipzig, Germany	[f] $SS = 45.0 - 6.82 \cdot T_w + 0.259 \cdot T_w^2$	$\delta_{SS} = 0.05 \cdot \sqrt{SS}$

[a] SN is the serial number of the instrument. Since LACIS is unique, this is not relevant for the Leipzig instrument.

[b] SS_{nom} is the "nominal" supersaturation computed from measurements of the difference between the bottom and top plate temperatures and the top plate temperature according to the chamber model of Katz and Mirabel (1975).

[c] During LExNo the Mainz instrument was operated with a 0.45 liter per minute sheath flow and a 0.05 liter per minute aerosol flow. The temperature at the column entrance was set at 22.6 ^{o}C.

[d] Here ΔT is the difference between temperatures measured near the inlet and exit of DMT column (Rose et al., 2008)

[e] During LExNo the Leipzig instrument was operated with a 4 liter per minute sheath flow, a 0.08 liter per minute aerosol flow and with the dew point of the aerosol and sheath flows set at 19.0 ^{o}C.

[f] This is a fit of the LExNo calibration data.

Table 2 – LExNo experiments and intra-experiment SS_c relative standard deviations

Aerosol Type	Synthesis Method	Number of Experiments	Participating Instruments [a]	SS_c Relative Standard Deviation [b]
Ammonium Sulfate	Spray Atomization	5	LAR, COP, MAI, LEI	0.01, 0.02, 0.04, 0.01
Levoglucosan	Spray Atomization	3	LAR, COP, MAI, LEI	0.06, 0.10, 0.14
Soot-Uncompacted-Levoglucosan	Thermal Condensation	6	LAR, COP, MAI, LEI	0.05, 0.10, 0.06, 0.03, 0.02, 0.08
Soot-Uncompacted-Ammonium Sulfate	Thermal Condensation	5	LAR, COP, MAI, LEI	0.10, 0.08, 0.10, 0.04
Soot-Compacted-Ammonium Sulfate	Thermal Condensation	5	COP, MAI, LEI	0.03
Soot-Compacted-Levoglucosan	Thermal Condensation	3	COP, MAI, LEI	0.03, 0.06, 0.10

[a] LAR = Laramie, COP = Copenhagen, MAI = Mainz and LEI = Leipzig

[b] Derived as $\sigma / \bar{x}$ where the denominator is the average of SS_c ($\bar{x} = \frac{1}{N}\sum_{0}^{N-1} x_i$), the numerator is $\sigma = \sqrt{\frac{1}{N-1}\sum_{0}^{N-1}(x_i - \bar{x})^2}$), and N is the number of instruments participating in an experiment. A value of $\sigma / \bar{x}$ is shown for experiments with N greater than 2.

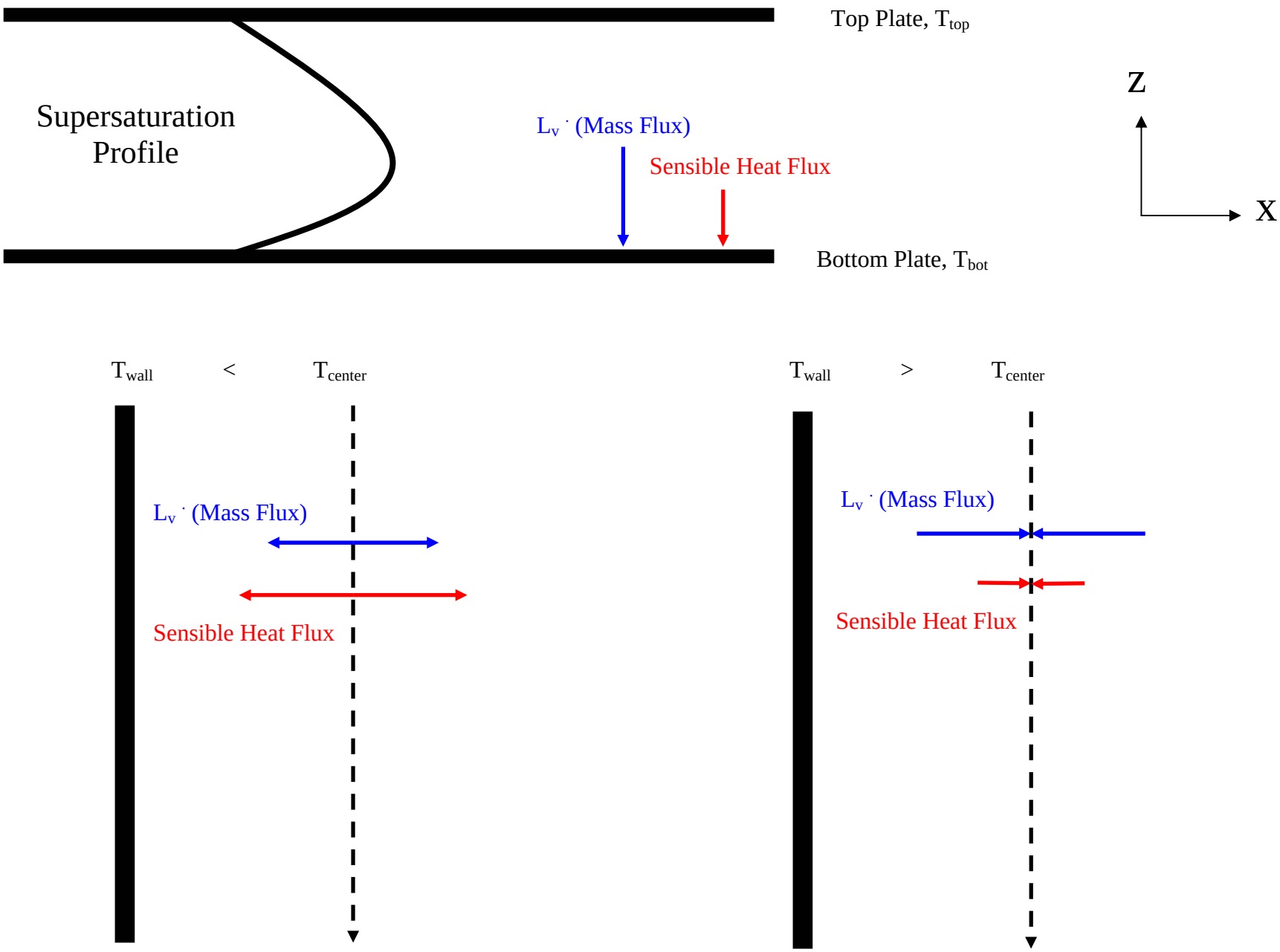

Figure 0 – Schematic vertical crossections of the Laramie (top), the Leipzig (bottom left) and the Mainz (bottom right) CCN chambers

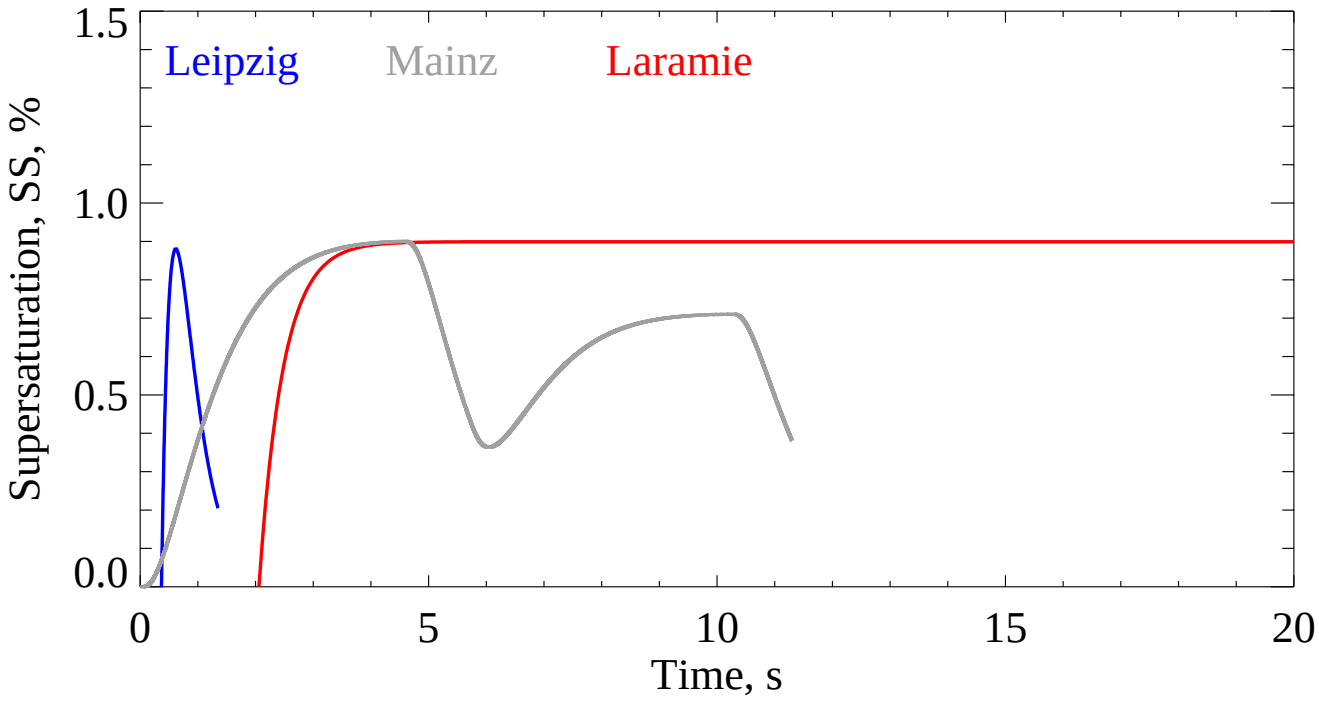

Figure 1 – Time-dependent chamber supersaturations based on models of the Leipzig, Mainz and Laramie CCN chambers. In the case of the Leipzig and Mainz instruments the supersaturation along the tube centerline is reported, starting at the tube entrance and ending at the tube exit. In the case of the Laramie CCN the supersaturation halfway between the top and bottom plates is reported, starting at the time the chamber is isolated and ending after the 20 s activation detection interval.

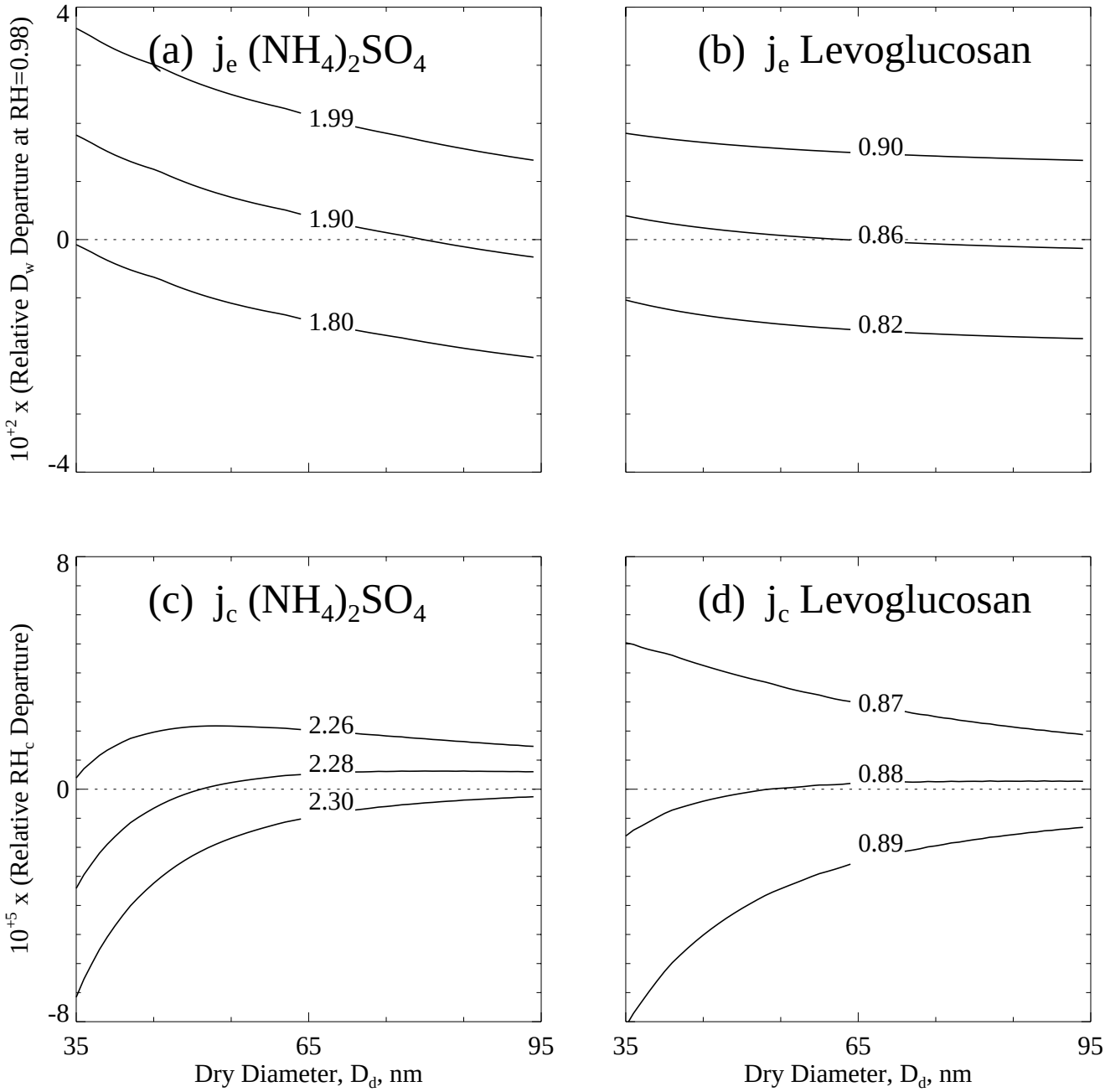

Figure 2 – Departure the working and exact Köhler models. The tuning parameter (either j_e or j_c) is shown labeling the middle line presented in each panel. Results obtained using a j_e value either 5% larger or 5% smaller is indicated in panels 2a and 2b. Results obtained using a j_c value either 1% larger or 1% smaller is indicated in panels 2c and 2d.

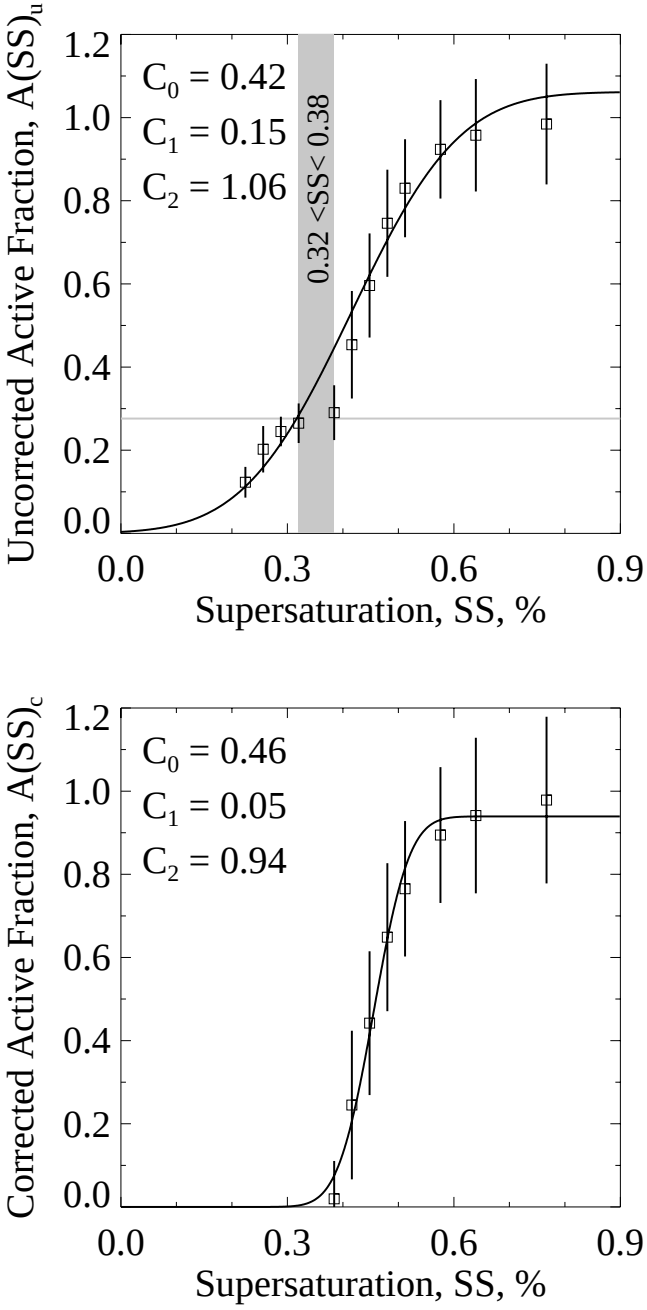

Figure 3 – Uncorrected active fraction plotted versus supersaturation (top panel) and corrected active fraction versus supersaturation (bottom panel). Data is from the Laramie CCN, LExNo experiment number #55. The test particles are composed of pure levoglucosan.

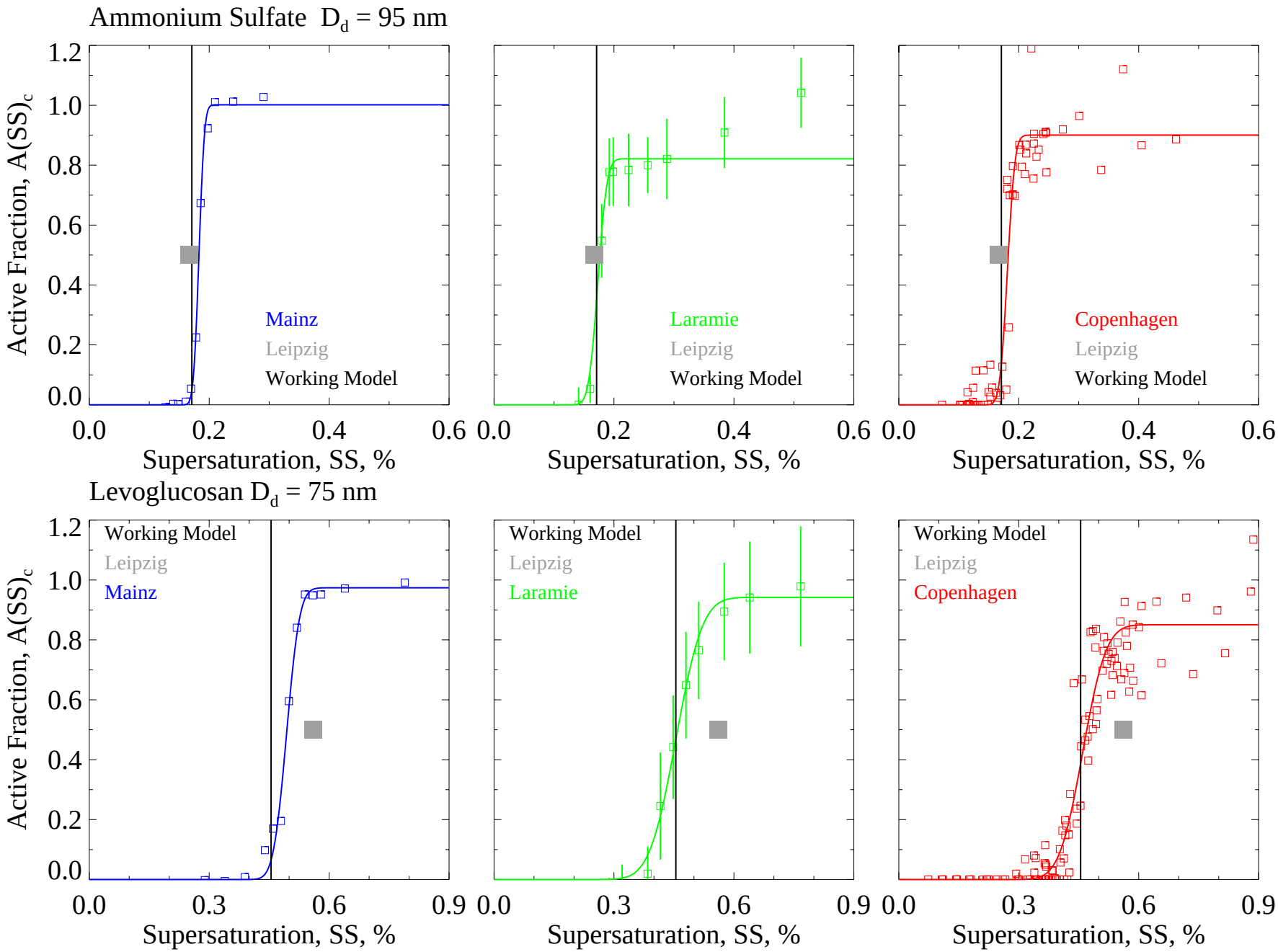

Figure 4 – Top, active fraction versus supersaturation; 95 nm diameter ammonium sulfate particles synthesized by spray atomization. Bottom, active fraction versus supersaturation; 75 nm diameter levoglucosan particles synthesized by spray atomization.

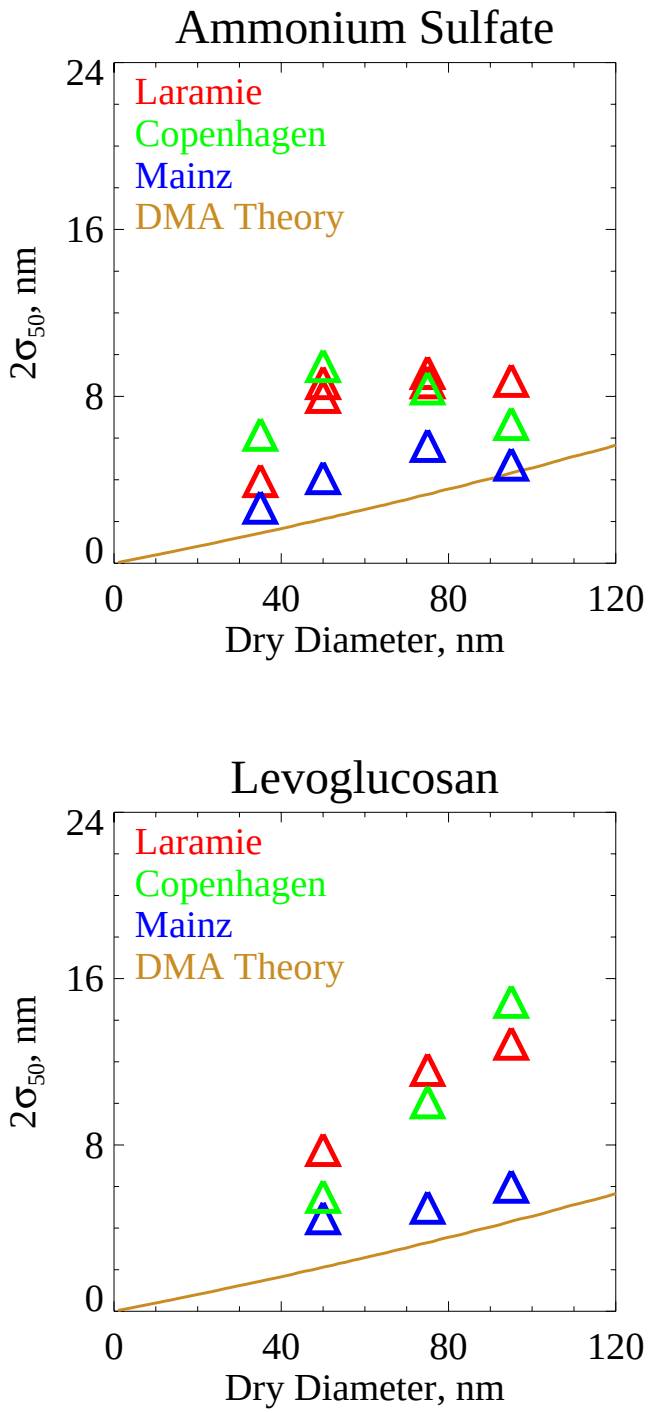

Figure 5 - The width of the test particle size distribution, at relative amplitude 0.61, derived from CCN measurements of the active fraction. The theoretical curve is based on Knutson and Whitby (1975) and corresponds to aerosol-to-sheath flow rate ratio used during LExNo (1-to-10), a mean free path for air (65.1 nm) and a Cunningham slip correction factor (Equation 8.34 in Seinfeld and Pandis, 1998).

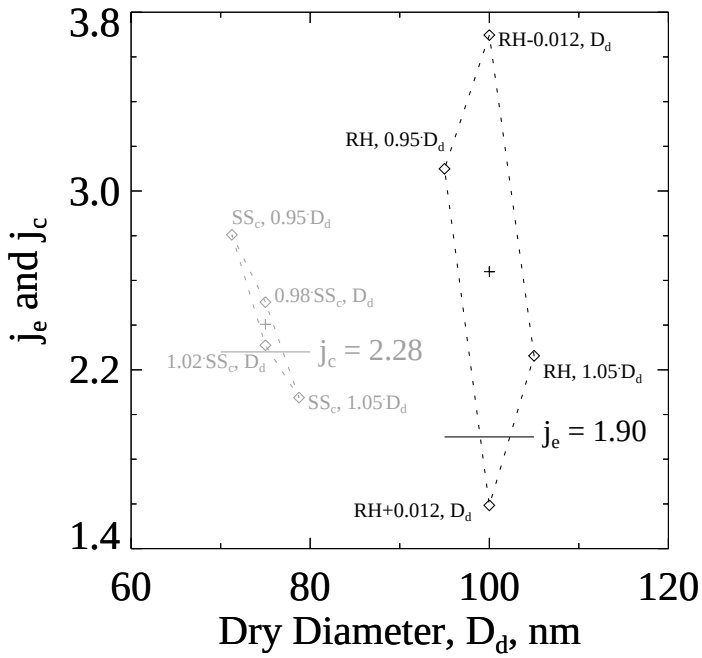

Figure 6 – On the left, an instrument-defined value of j_c (indicated by the "+"), the rhomb-shaped error region discussed in the text and the value of j_c which forces the best possible agreement between the working and exact Köhler models. Used in the calculation of j_c is the average of the four SS_c determinations from LExNo measurements of a aerosol composed of 75 nm ammonium sulfate particles. On the right, an instrument-defined value of j_e (indicated by the "+"), the rhomb-shaped error region defined in the text and the value of j_e which forces the best possible agreement between the working and exact Köhler models. Used in the calculation of j_e is the fractional *RH* (0.977) and wet diameter (279 nm) from Hennig et al. (2005, final row of their Table 2). The error in fractional relative humidity is taken from Hennig et al. The test aerosol was composed of 100 nm dry diameter ammonium sulfate particles.

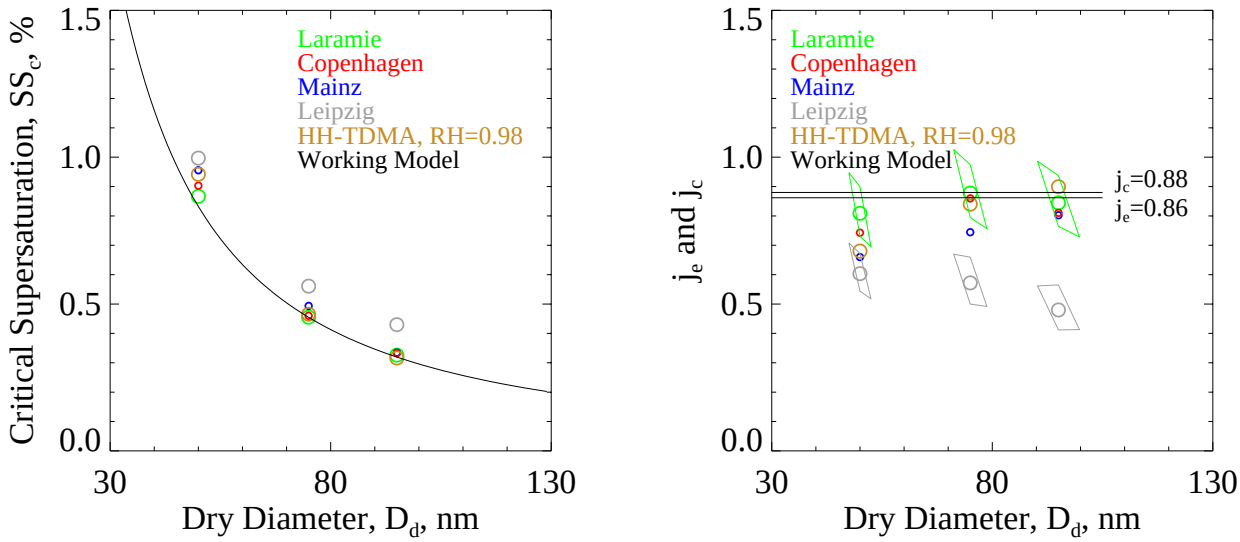

Figure 7 –Left, critical supersaturation values based on CCN and HH-TDMA measurements of levoglucosan particles prepared by spray atomization. Right, instrument-defined values of j_c and j_e, the rhomb-shaped error region for the Laramie and Leipzig CCN instruments, and horizontal lines showing the tuned values j_c and j_e.

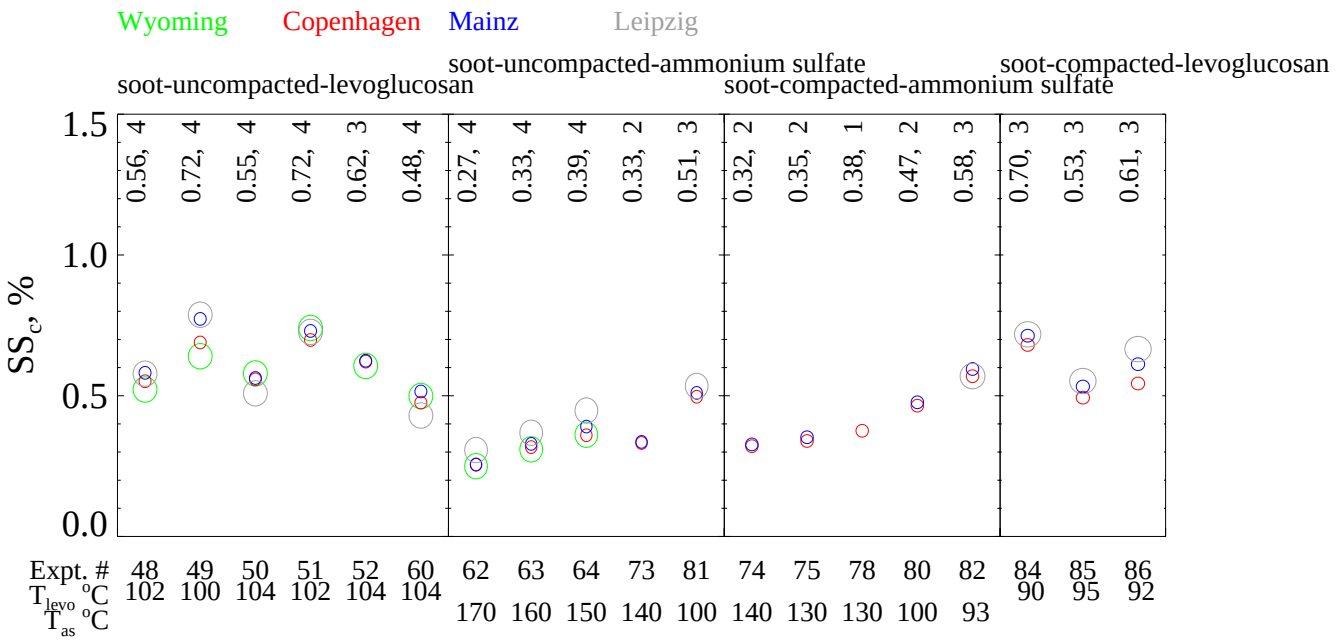

Figure 8 – Critical supersaturation values for internally-mixed soot-ammonium sulfate and soot-levoglucosan particles. Above each panel is indication of whether, or not, the soot particles were compacted in the propanol compactor prior to entry into the ammonium sulfate or levoglucosan ovens (section 3.1). Below each panel is the experiment number, the temperature of the levoglucosan oven and the temperature of the ammonium sulfate oven.

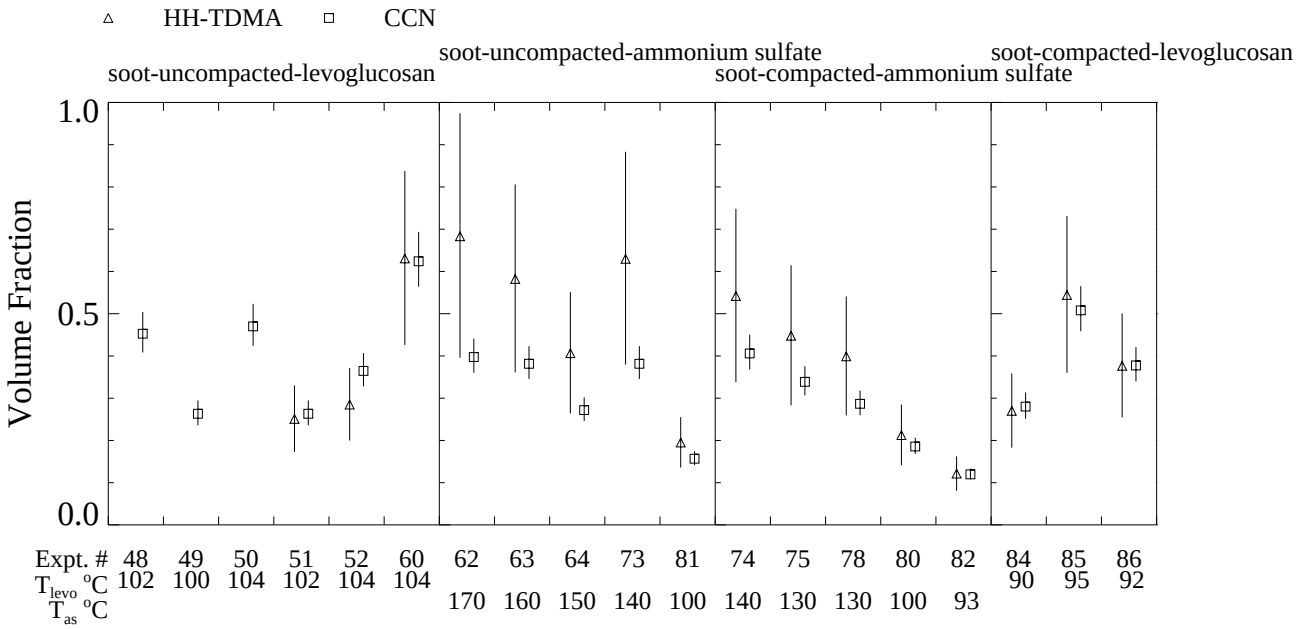

Figure 9 – As in Figure 8, but for hygroscopic volume fraction (ε). Error limits on the HH-TDMA points come from Equation 5c initialized with RH -0.012 to RH +0.012 where RH is the fractional relative humidity inside the high-humidity electrostatic classifier of the HH-TDMA. Error limits on the CCN points come from Equations 5a and 5b initialized with $0.95 \cdot SS_c$ and $1.05 \cdot SS_c$.

References

Andreae, M.O., E.V.Browell, M.Garstang, G.L.Gregory, R.C.Harriss, G.F.Hill, D.J.Jacob, M.C.Pereira, G.W.Sachse, A.W.Setzer, P.L.Silva Dias, R.W.Talbot, A.L.Torres and S.C.Wofsy, Biomass-Burning Emissions and Associated Haze Layers over Amazonia, J. Geophys. Res., 93, 1509–1527, 1988

Bilde, M. and B. Svenningsson, CCN activation of slightly soluble organics: the importance of small amounts of inorganic salt and particle phase. Tellus, 56B, 128-134, 2004

Brechtel, F.J. and S.M.Kreidenweis: Predicting particle critical supersaturation from hygroscopic growth measurements in the humidified TDMA, Part I: Theory and sensitivity studies, J.Atmos.Sci., 57(12), 1854-1871, 2000

Boucher, O. and T. L. Anderson. General circulation model assessment of the sensitivity of direct climate forcing by anthropogenic sulfate aerosols to aerosol size and chemistry, J Geophys Res, 100(D12), 26117-26134, 1995

Chan, M.N., S.M.Kreidenweis and C.K.Chan, Measurements of the hygroscopic and deliquescence properties of organic compounds of different water solubilities in water and their relationship with cloud condensation nuclei activities, 42, 3602-3608, 2008

Chýlek, P. and Wong, J.G.D., Erroneous use of the modified Köhler equation in cloud an aerosol physics applications, *J. Atmos. Sci.*, 55, 1473–1477, 1998

Gras, J.L., CN, CCN and particle size in the southern ocean air at Cape Grim. Atmos. Res., 35, 233-251, 1995

Hennig, T., A.Massling, F.J.Brechtel and A.Wiedensohler, A tandem DMA for highly temperature-stabilized hygroscopic particle growth measurements between 90% and 98% relative humidity, J.Aerosol Sci., 36(10), 1210-1223, 2005

Hudson, J.G. and X.Y.Da, Volatility and size of cloud condensation nuclei, J.Geophys.Res., 101, 4435-4442, 1996

Fitzgerald, J.W., On the computation of steady-state supersaturations in thermal diffusion chambers, J.Atmos.Sci., 29, 779-781, 1972

Katz, J. L. and Mirabel, P., Calculation of supersaturation profiles in thermal diffusion cloud chambers. J. Atmos. Sci., 32(3), 646–652, 1975

Kiselev, A. and Wex, H. and Stratmann, F. and Nadeev, A. and Karpushenko, D.: White-light optical particle spectrometer for in situ measurement of condensational growth of aerosol particles. Appl. Opt., 44, 4693-4701, 2005

Knutson, E. O. and Whitby, K. T., Aerosol classification by electric mobility: Apparatus, theory, and applications, J. Aerosol. Sci., 6, 443–451, 1975

Kreidenweis, S.M., M.D.Petters and P.J.DeMott, Single-parameter estimates of aerosol water content, Environ. Res. Lett., 3, 1-7, 2008

Lance, S., Medina, J., Smith, J. N., and Nenes, A., Mapping the Operation of the DMT Continuous Flow CCN Counter, Aerosol Science & Technology, 40, 242-254, 2006

Lehmann, K., A.Massling, A.Tilgner, S.Mertes, D.Galgon and A.Wiedensohler, Size-resolved soluble volume fractions of submicrometer particles in air masses of different character, Atmos.Environ., 39, 4257-4266, 2005

Lightly, J.S., J.M.Vernath and A.F.Sarofim, Combustion aerosols: Factors govering their size and composition and implications for human health, J.Air Waste Manag. Assoc., 50, 1565-1618, 2000

Low, R.D.H., A generalized equation for the solution effect in droplet growth, J. Atmos. Sci., 26, 1345-1346, 1969a

Low, R.D.H., Reply, J. Atmos. Sci., 26, 608-611, 1969b

McDonald, J.E., Erroneous cloud-physics applications of Raoult's Law, J.Meteor., 10, 68-70, 1953

McMurry, P. H. and M. R. Stolzenburg, On the Sensitivity of Particle-Size to Relative-Humidity for Los-Angeles Aerosols, Atmos Environ, 23(2), 497-507, 1989

Mita, A., A reexamination of the formula expressing the equilibrium water vapor pressure over an aqueous solution droplet, J.Met.Soc.Japan, 57, 79-83, 1979

Nenes, A., P.Y.Chuang, R.C.Flagan, and J.H. Seinfeld, A theoretical analysis of cloud condensation nucleus (CCN) instruments. J. Geophys. Res., 106, 3449–3474, 2001

Petters, M.D. and S.M.Kreidenweis, A single parameter representation of hygroscopic growth and cloud condensation nucleus activity, Atmos. Chem. Phys., 7, 1961-1971, 2007

Pruppacher, H. R. and J. D. Klett, *Microphysics of Clouds and Precipitation*, Kluwer, Dordrecht, 1997

Roberts, G. C., and Nenes, A., A Continuous-Flow Streamwise Thermal-Gradient CCN Chamber for Atmospheric Measurements, Aerosol Science & Technology, 39, 206-221, 2005.

Rose, D., Gunthe, S.S., Mikhailov, E., Frank, G.P., Dusek, U., Andreae, M.O., and Pöschl, U., Calibration and measurement uncertainties of a continuous-flow cloud condensation nuclei counter (DMT-CCNC): CCN activation of ammonium sulfate and sodium chloride aerosol particles in theory and experiment, Atmos. Chem. Phys., 8, 1153-1179, 2008

Saxena, V.K., J.N.Burford and J.L.Kassner Jr., Operation of a thermal diffusion chamber for measurements on cloud condensation nuclei, J.Atmos.Sci., 27, 73-80, 1970

Seinfeld, J. H. and Pandis, S. N., Atmospheric Chemistry and Physics, John Wiley and Sons, 1326 pages, 1998

Snider, J.R., S.Guibert, J.-L. Brenguier, and J.-P.Putaud, Aerosol activation in marine stratocumulus clouds: Part – II Köhler and parcel theory closure studies. J. Geophy. Res., 108, 8629, doi:10.1029/2002JD002692, 2003

Snider, J.R., M.D.Petters, P.Wechsler and P.Liu, Supersaturation in the Wyoming CCN Instrument, J. Atmos. Oceanic Technol., 23, 1323-1339, 2006

Stratmann, F., Kiselev, A., Wurzler, S., Mendisch, M., Heinzenberg, J., Charlson, R.J., Diehl, K., Wex, H., and Schmidt, S.: Laboratory studies and numerical simulations of cloud droplet formation under realistic supersaturation conditions, J. Atmos. Ocean. Tech., 21, 876-887, 2004

Subramanian,R.S., http://web2.clarkson.edu/subramanian/ch560/notes/graetz%20problem.pdf, 2009

Svenningsson, B., J.Rissler, E.Swietlicki, M.Mircea, M.Bilde, M.C. Facchini, S.Decesari, S.Fuzzi, J.Zhou, J.Mønster, and T.Rosenørn, Hygroscopic growth and critical supersaturations for mixed aerosol particles of inorganic and organic compounds of atmospheric relevance, Atmos. Chem. Phys., 6, 1937-1952, 2006

Textor, C., M.Schulz, S.Guibert, S.Kinne, Y.Balkanski, S.Bauer, T.Berntsen, T.Berglen, O.Boucher, M.Chin, F.Dentener, T.Diehl, R.Easter, H.Feichter, D.Fillmore, S.Ghan, P.Ginoux, S.Gong, A.Grini, J.Hendricks, L.Horowitz, P.Huang, I.Isaksen, I.Iversen, S.Kloster, D.Koch, A.Kirkevåg, J.E.Kristjansson, M.Krol, A.Lauer, J.F.Lamarque, X.Liu, V.Montanaro, G.Myhre, J.Penner, G.Pitari, S.Reddy, Ø.Seland, P.Stier, T.Takemura, and

X.Tie, Analysis and quantification of the diversities of aerosol life cycles within AeroCom Atmos. Chem. Phys., 6, 1777-1813, 2006

Tao, Y. and P.H.McMurry, Vapor pressures and surface free energies of C14-C18 Monocarboxylic acids and C5 and C6 dicarboxylic Acids, Environ.Sci.Technol., 23, 1519-1523, 1989

Twomey, S., Atmospheric Aerosols, Elsevier, 302 pp., New York, 1977

Warner, J. and S.Twomey, The production of cloud nuclei by cane fires and the effect on cloud droplet concentration, J. Atmos. Sci., 24, 704-706, 1967

Wex, H., A. Kiselev, M. Ziese, and F. Stratmann, Calibration of LACIS as a CCN detector and its use in measuring activation and hygroscopic growth of atmospheric aerosol particles, Atmos. Chem. Phys., 6, 4519-4527, 2006

Wex, H., T.Hennig, I.Salma, R.Ocskay, A.Kiselev, S.Henning, A.Massling, A.Wiedensohler and F. Stratmann, Hygroscopic growth and measured and modeled critical supersaturations of an atmospheric Hulis sample, Geophys. Res. Lett., 34, L02818, doi:10.1029/2006GL028260, 2007

Wexler, A.S. and S.L.Clegg: Atmospheric aerosol models for systems including the ions H^+, NH_4^+, Na^+, SO_4^{2-}, NO_3^-, Cl^-, Br^-, and H_2O, J.Geophys.Res., 107, 4207, doi:10.1029/2001JD000451, 2002